frontiers | Frontiers in Energy Research

TYPE Original Research
PUBLISHED 22 August 2024
DOI 10.3389/fenrg.2024.1404791

OPEN ACCESS

EDITED BY
Davide Astolfi,
University of Perugia, Italy

REVIEWED BY
Zhiping Tian,
Chinese Academy of Sciences (CAS), China
Igor Esau,
Nansen Environmental and Remote Sensing Center (NERSC), Norway
Rui Chang,
China Meteorological Administration, China

*CORRESPONDENCE
Xiaoli Guo Larsén,
xgal@dtu.dk

RECEIVED 21 March 2024
ACCEPTED 07 August 2024
PUBLISHED 22 August 2024

CITATION
Larsén XG, Imberger M and Hannesdóttir Á (2024) The impact of Climate Change on extreme winds over northern Europe according to CMIP6.
Front. Energy Res. 12:1404791.
doi: 10.3389/fenrg.2024.1404791

The impact of Climate Change on extreme winds over northern Europe according to CMIP6

Xiaoli Guo Larsén*, Marc Imberger and Ásta Hannesdóttir

Department of Wind and Energy Systems, Technical University of Denmark, Roskilde, Denmark

We study the possible effect of climate change on the extreme wind over northern Europe using data from 18 models of the Sixth Phase of the Coupled Model Intercomparison Project (CMIP6) and the high-emission Shared Socioeconomic Pathway 5-8.5 (SSP585) scenario. We use the spectral correction method to correct the 6-hourly wind speeds and calculate the 50-year wind at an equivalent temporal resolution of 10 min, consistent with the International Electrotechnical Commission (IEC) standard. We obtain the possible effect of climate change through the comparison of the extreme wind parameters, including the 50-year wind and the 95%-percentile of the wind speed, and the change in turbine class at 50 m, 100 m and 200 m, between a near future period (2020–2049) and the historic period (1980–2009). The analysis shows an overall increase in the extreme winds in the North Sea and the southern Baltic Sea, but a decrease over the Scandinavian Peninsula and most of the Baltic Sea. However, the suggested change is not significant enough to conclude whether higher or lower classes of turbines will be needed in this area in the future.

KEYWORDS

climate change, 50-year wind, CMIP6 data, IEC standard, reanalysis data

1 Introduction

Extreme winds can cause great loss to society and the 50-year wind, U_{50}, a common measure of extreme winds, is one of the most important siting parameters that must be estimated when planning regional wind energy development. An accurate estimation of the extreme wind can help to harvest more electricity from winds, while avoiding placing the turbines in dangerous places, and to avoid over-designing of the wind turbines; it is directly related to the Levelized Cost of Energy (LCOE) and the implied cost of climate mitigation.

The scale and speed of wind energy development and deployment have never been so great and it will continue in the future (GWEC, 2022), but we also live in a world where climate is changing potentially affecting wind farm siting parameters like the 50-year return wind. Therefore, it is a relevant question to ask how climate change will impact extreme winds in the future and what this change implies for the cost of wind energy planning and development.

Extreme winds have not been studied as extensively as some other meteorological parameters such as extreme temperature and precipitation. The studies of extreme winds have also mostly been done though historical data from reanalysis and regional downscaling. Reanalysis data has been a popular choice for extreme wind estimation due to its global coverage and long-term availability, including European Centre for Medium-Range Weather Forecasts (ECMWF) reanalysis ERA-40 (e.g., Della-Marta et al., 2009), reanalysis

from the National Centers for Environmental Prediction and the National Center for Atmospheric Research (NCEP/NCAR) (e.g., Larsén and Mann, 2009), the National Oceanic and Atmospheric Administration (NOAA) 20th century reanalysis (e.g., Donat et al., 2011), the 5th generation reanalysis from the ECMWF, ERA5 (e.g., Pryor and Bartelmie, 2021; Imberger and Larsén, 2022), Climate Four-Dimensional Data Assimilation (CFDDA) (e.g., Hansen et al., 2016), Climate Forecast System Reanalysis (CFSR) (e.g., Larsén and Kruger, 2014) and Modern-Era Retrospective analysis for Research and Applications version 2 MERRA2 (e.g., Imberger and Larsén, 2022). The temporal resolution of these data ranges from 1 to 6 h, and the spatial grid spacing from about 25 km to a couple of hundreds of kilometers. This resolution is too coarse and not ideal for site-specific extreme wind calculations. Using data from mesoscale model simulations is expected to improve the extreme wind estimation, as shown in, e.g., Bastine et al. (2018) and Larsén et al. (2021), where data from the Weather Research and Forecasting (WRF) model with spatial grid spacing of 3 km were used. The only global coverage of extreme wind that has applied microscale modeling with spatial grid spacing of 275 m has been created within the Global Atlas for Siting Parameters (GASP) project (Larsén et al., 2022). The above-mentioned studies look at issues related to the calculation of extreme winds through model data of different spatial and temporal resolution, and focus on the estimation of extreme winds using historical data, rather than the impact of climate change.

In recent decades, Regional Climate Models (RCMs) have been used to study the impact of climate change on extreme wind. However, these studies founded on several generations of RCMs do not seem to have reached a consensus. These studies include, for example, the PRUDENCE project (Prediction of Regional Scenarios and Uncertainties for Defining European climate change Risks and Effects), a EU Framework Program project that ended in 2004 (WCRP Working Group on Coupled Modeling (WGCM), 2004), ENSEMBLES (Ensemble-Based Predictions of climate changes and Their Impacts), a successor to PRUDENCE which finished in 2009 (van der Linden and Mitchell, 2009) and CORDEX (Coordinated Regional Downscaling Experiment, Giorgi and Gutowski, 2015), based on data known from the Fifth Phase of the Coupled Model Intercomparison Project (CMIP5; Taylor et al., 2012). The RCMs included in the PRUDENCE project have a spatial grid spacing of 50 km, ENSEMBLES 25 km and Euro-CORDEX 12 km. With PRUDENCE, Beniston et al. (2007) (with both high and low emission scenarios A2 and B2), Schwierz et al. (2010) (with SRES[1] A2 scenario), and Rockel and Woth (2007) (also with SRES A2 scenario) studied the climate change on extreme wind using the 90th, 98th, and 99th percentiles of wind speed, as well as the gust and the T–year return wind speed for the period 1961–1990 vs. 2071–2100. They found that these models suggest an increase in extreme wind in Central Europe in the future due to climate change. With ENSEMBLE, Donat et al. (2011) (with SRES A1B scenario) analyzed the 98th percentile of wind speed and found an increase in Northern Europe and a decrease in the Mediterranean Sea; Pryor et al. (2012) (with SRES A1B scenario) analyzed U_{50} and found similar change in Northern Europe in line with findings by Donat et al. (2011) and Clausen et al. (2012) (with SRES A1B scenario) analyzed four ensemble model members and calculated the 90th, 95th and 99th percentiles, U_{50} and the linear trend at hub height of 100 m, and found that in Europe, there is no significant change in U_{50} in majority of the grid cells by the middle of the century, while towards the end of the century, there is an increasing number of grid cells that show increases in U_{50} larger than the natural variability. With Euro-CORDEX, Outten and Sobolowski (2021) with the Representative Concentration Pathway 8.5 (RCP8.5) scenario calculated 10, 20, 30, 50, and 100-year return wind values for Europe for three periods 2011–2040, 2041–2070, and 2071–2100 and they found an overall increase in extreme wind in the future, for both Northern and Southern Europe. Comparison to ENSEMBLE data estimations, Outten and Sobolowski (2021) found that the 12 km resolution CORDEX data provides more details over complicated landscape, e.g., land and coastal areas, with enhanced extreme events. The typical resolution of RCMs, which is on the order of tens of kilometers on hourly basis, is still not high enough for the purpose of site specific estimation of extreme wind, due to the ever-present smoothing effect in numerical models (Larsén et al., 2012). However, these data are still useful to identify trends and changes in the extreme wind estimation.

To follow up these investigations, this study examines the possible climate change impact on the extreme winds using the new, CMIP6 data, here particularly the 50-year wind U_{50} over a historical period (1980–2009) and a near future period (2020–2049). To assist the analysis of U_{50}, the 95% quantile of the wind speed Q_{95} is used too. The CMIP6 project is the sixth phase and most recent phase of the CMIPs (Eyring et al., 2016). It used World Climate Research Programme (WCRP) Grand Science Challenges as the scientific backdrop of its experiment design. These Grand Science Challenges constitute a main component of the WCRP strategy to accelerate progress in climate science (Brasseur and Carlson, 2015), with one of the seven subjects particularly on climate extremes: "assessing climate extremes, what controls them, how they have changed in the past, and how they might change in the future." A parallel study, Hahmann et al. (2022), used this data set to examine the effect of climate change on wind resources in northern Europe.

The CMIP6 data are available every 6 h, which is a resolution too coarse for the purpose of calculating the extreme wind, according the IEC standard, where a temporal resolution of 10 min is needed (IEC, 2019). To relate our calculation and analysis to the IEC standard for turbine design, and hence to be able to address the impact of climate change from the perspectives of wind energy application, we downscale the CMIP6 time series of wind speed in the temporal domain using a fast and simple spectral model that is well established for wind energy applications. This method, called the spectral correction method, corrects the CMIP6 time series to an equivalent 10-min temporal resolution and it is introduced in Section 2.3. Data, including CMIP6 and reanalysis data, are introduced in Section 2, followed by the results in Section 3. The discussion of the results and the conclusions are in Section 4 and Section 5, respectively.

For readability, a list of Abbreviations is provided at the end of this paper.

1 Special Report on Emissions Scenarios (SRES) published by the Intergovernmental Panel on climate change (IPCC).

2 Data and methods

We use the output from CMIP6 models to assess the climate change impact on the extreme wind over two periods: the historical period (his-Period, 1980–2009) and the near future period (fut-Period, 2020–2049) from the CMIP6 historical and SSP585 simulations, respectively (Eyring et al., 2016). These two periods are relevant for a turbine's life time of 20–30 years for a wind farm being planned in 2020. When assessing the CMIP6 data quality, we use three reanalysis data sets and measurements from the three FINO (Forschungsplattformen in Nord-und Ostsee) masts in the North Sea and the Baltic Sea for comparison with CMIP6 from his-Period.

The CMIP6 data are introduced in Section 2.1 and the reanalysis data in Section 2.2. When calculating U_{50}, both CMIP6 and the reanalysis data will be processed using the spectral correction method, which is described in Section 2.3. Q_{95} is used along with U_{50} when assessing climate change impact and it is defined as the wind speed value corresponding to the 95% highest wind sample collection of the original CMIP6 data. Q_{95} is a strong wind index, however it is not a design parameter and there is no temporal resolution associated with its definition. Accordingly, the spectral correction is not applied to Q_{95}. Following that, in Section 2.4, data and the comparison of the estimates of U_{50} from three FINO masts is briefly introduced. In Section 2.5, we introduce the approaches for addressing the statistical significance in the change of U_{50} between fut-Period and his-Period.

2.1 The CMIP6 data

Consistent with the study of wind resources using CMIP6 data in Hahmann et al. (2022), we use the 18 models listed in Table 1 for the high emission scenario SSP585. Among the many CMIP6 models these 18 are chosen for the same reason as given in Hahmann et al. (2022): the availability of model outputs of surface pressure, temperature and humidity in addition to the wind components u and v at the raw model level for the simulations of the historical (1980–2014) and future (2015–2050) scenarios. With the information of the profile of temperature and humidity and the surface pressure, we can compute the height of the model's sigma levels and hence interpolate the wind speed from these levels to the desired heights above ground level, namely, at 50 m, 100 m, and 200 m. These heights are relevant for modern turbine sizes. The vertical interpolation of wind speed applies logarithmic dependence of wind speeds on height for these heights. The reason of choosing SSP585, instead of other scenarios, is to take advantage of its extreme, high emission, and hence to study the likely higher climate change impact.

To reduce the data download volume, we follow Hahmann et al. (2022) and crop the CMIP6 model data domain to approximately cover the area −10 – 30°E and 50 – 70°N. The 18 models are labeled with numbers in Table 1, together with the corresponding atmospheric model grid spacing and the number of vertical model levels. All data are available on 6-h basis. Details of these models can be found in the references. As the grid spacing of the 18 models is different, we interpolate all models to the reference grid from model 5 (with a grid spacing of 1.4 °) through a nearest-neighbor interpolation. Model 5, together with model 6 and 10, has the highest quality scores as will be shown in Section 3.1.2. To avoid filtering out information relevant for extreme wind studies from models of higher spatial resolution, we chose not to use the most coarse spatial resolution for the grid interpolation as often done in climate studies. It is of course a relevant question how the results and conclusions are affected by the choice of the reference model grid points and the choice the interpolation. In Supplementary Appendix S5, a detailed investigation is carried out using two other reference model grid points, with one as the most coarse and one as the highest spatial resolution. In addition, we add the bi-linear interpolation method.

2.2 The reanalysis data

The reanalysis data is used to assess the reliability of the CMIP6 wind speeds in describing extreme winds in the historic period in this region through a qualitative description of the spatial distribution and patterns of U_{50}.

Three reanalysis data sets are used: 1) the CFSR (Saha et al., 2010) available at hourly temporal resolution with a grid spacing of about 40 km; 2) the MERRA2 (Gelaro et al., 2017) available hourly with a grid spacing of 0.5 × 0.625°, and 3) the ERA5 (Hersbach et al., 2020) available hourly with a grid spacing of about 27 km. We calculate U_{50} using the his-Period with the three data sets with the spectral correction method.

Wind speed diagnostics are available at different heights in the three reanalysis: 10 m (CFSR), 10 m and 50 m (MERRA2), and at 10 m and 100 m (ERA5). A single common height for comparison with hub height would be ideal. However, extrapolating wind speeds from a height, i.e., 10 m or 50 m, to a typical modern turbine hub height (~100 m) uses several assumptions (e.g., Hahmann et al., 2022), and thus considerable uncertainty is added when considering the magnitude of the wind speed. Therefore, we avoid addressing the absolute value at a given point on the grid and focus on the spatial patterns of U_{50} based on the values at 10 m where all three reanalysis data are available.

2.3 The spectral correction method and the annual maximum method

The IEC standard requires that the 50-year return wind estimate are based on time series equivalent to a temporal resolution of 10 min. Thus, we cannot use the estimation of U_{50} directly from the 6-hourly CMIP6 data to refer to the IEC standard. The poor temporal sampling in addition to numerical smoothing effects due to the spatial discretization means that significant variability is missed compared to time series with a sampling rate every 10-min; the variability is essential for the estimation of the extreme wind (Larsén and Mann, 2006; Larsén et al., 2012). This issue is illustrated in Figure 1. When being presented as power spectrum $S(f)$ as a function of frequency f, the original 6-hourly time series shows a fast decrease of energy from about $f = 1$ day^{-1} to very little energy at $f = 2$ day^{-1}, and no energy for $f > 2$ day^{-1} (gray curve) compared with the red curve (based on measurements) in the same range. The missing energy in this high frequency range affects the calculation

TABLE 1 Models in the CMIP6 archive used in this study.

No.	Model	Approx. grid spacing	Number of vertical levels	References
1	ACCESS-CM2	1.25° × 1.875°	85	Tilo et al. (2020)
2	CanESM5	2.8125° × 2.79°	49	Swart et al. (2019)
3	CESM2	1.25° × 0.94°	32	Danabasoglu et al. (2020)
4	CMCC-CM2-SR5	1.25° × 0.94°	30	Cherchi et al. (2019)
5	CNRM-CM6-1	1.4° × 1.4°	91	Voldoire et al. (2019)
6	CNRM-ESM2-1	1.4° × 1.4°	91	Séférian et al. (2019)
7	HadGEM3-GC31-LL	1.875° × 1.25°	85	Sellar et al. (2020)
8	HadGEM3-GC31-MM	0.833° × 0.556°	85	Sellar et al. (2020)
9	IPSL-CM6A-LR	2.5° × 1.27°	91	Boucher et al. (2020)
10	MIROC6	1.4° × 1.4°	81	Tatebe et al. (2019)
11	MIROC-ES2L	2.8125° × 2.79°	40	Hajima et al. (2020)
12	MPI-ESM1-2-HR	1.875° × 1.865°	47	Müller et al. (2018)
13	MPI-ESM1-2-LR	0.9375° × 0.935°	85	Mauritsen et al. (2019)
14	MRI-ESM2-0	1.125° × 1.121°	80	Kawai et al. (2019)
15	NESM3	1.875° × 1.865°	47	Yang et al. (2020)
16	NorESM2-LM	2.5° × 1.895°	32	Seland et al. (2020)
17	NorESM2-MM	1.25° × 0.942°	32	Seland et al. (2020)
18	UKESM1-0-LL	1.875° × 1.25°	85	Sellar et al. (2020)

of the extreme wind significantly, and the deficit can be derived straightforwardly and mathematically. If we assume that the once-per-year exceedance of the wind speed follows a Poisson process, at a threshold for the rate of once-per-year, such a distribution of the exceedance can be simplified as a Gaussian process, and accordingly, the maximum wind that occurs once a year, $\overline{U}_{\max}$, can be derived as a function of the zero- and second-order spectral moments m_0 and m_2:

$$\overline{U}_{\max} = \overline{U} + \sqrt{m_0}\sqrt{2\ln\left(\sqrt{\frac{m_2}{m_0}}T_0\right)}, \tag{1}$$

where $\overline{U}$ is the mean wind speed, T_0 is the basis period of 1 year and m_i is the ith spectral moment defined by

$$m_i = 2\int_0^\infty f^i S(f)\ df. \tag{2}$$

Please refer to Larsén et al. (2012) for details of the derivation. Equations 1, 2 show clearly that $\overline{U}_{\max}$ is significantly affected by the values of $S(f)$ at high frequencies through m_2. Thus, if we can correct the spectral tail, we can improve the calculation of $\overline{U}_{\max}$.

The spectral correction method uses the spectral model from Larsén et al. (2013) to estimate the tail of the distribution for $(1\,\text{day})^{-1} < f < 10^{-3}$ Hz:

$$S(f) = a \cdot f^{-5/3}, \tag{3}$$

where the value of the coefficient a is calculated from the spectrum of the model data: referring to Figure 1, if we take the value of S from the above equation at $f = 0.8$ day^{-1}, a can be obtained. The choice of where to start the replacement of the spectral tail depends on which frequency the modelled data reproduce the fluctuation. Exemplified Figure 1, we replace the tapered-out spectrum in gray for $f > 0.8$ day^{-1} with the red curve, Equation 3, for $0.8 < f < 72$ day^{-1}, where 72 day^{-1} is the Nyquist frequency of a time series with a temporal resolution of 10-min. In Larsén et al. (2022), a regression line was obtained to describe the power spectrum and frequency in the range of 0.6 – 0.9 day^{-1}, following the expected spectral behavior (Equation 3). Thus, it is not sensitive to use f_c in the range of 0.6 – 0.9 day^{-1}. We use this approach here too. Then we apply Equations 1, 2 with both the original and corrected spectra to obtain $\overline{U}_{\max,\text{orig}}$ and $\overline{U}_{\max,\text{corr}}$. The ratio of the two is used to correct the annual maximum values from the CMIP6 time series to the values equivalent to 10 min. The magnitude of the change

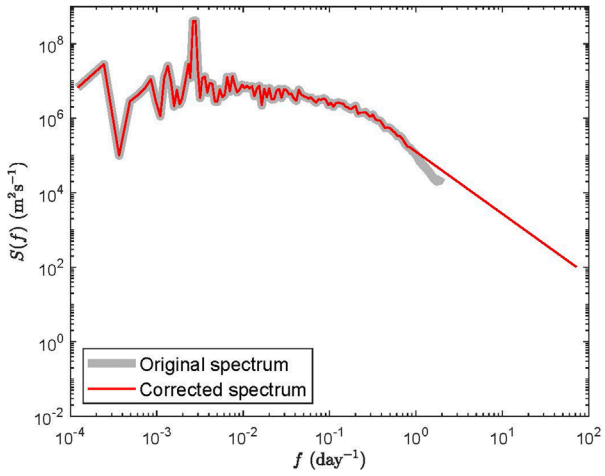

FIGURE 1
An example of the spectrum of the 6-hourly time series of wind speed at 100 m from the CNRM-CM6-1 model of historical period and the corrected spectrum to equivalent resolution of 10-min. The time series is from the location 56.7309°N, 9.84372°W.

from the spectral correction method depends on how smoothed the original time series is in comparison with what is expected of an observed 10-min time series, namely, the difference between the gray and red curves. For the example shown in Figure 1, U_{50} = 32.5 m s^{-1} from the raw CMIP6 data, and after the spectral correction, U_{50} = 42.8 m s^{-1}.

The spectral behavior is related to the energy transfer and cascade across atmospheric flow of different scales, following the law of physics. We assume the same set of physics laws in the future as in the historic data, and therefore do not introduce climate change in the spectra of the wind speed. This assumption should be reasonable, as demonstrated by the example of similar spectra from both the historical and future periods in Supplementary Figure S1, shown in Supplementary Appendix SA.

The spectral correction method has been applied in research and industry for U_{50} estimation. It was also used for creating the global atlas of siting parameters in Larsén et al. (2022) and validated with measurements from several continents (e.g., Larsén and Kruger, 2014; Hansen et al., 2016; Larsén et al., 2022). With this method, we can correct the annual wind maxima U_i^{max} (i = 1, n) from the CMIP6 time series to a temporal resolution equivalent to 10 min, where n = 30 as the number of years of the CMIP6 data.

The T-year return wind U_T for the Gumbel distribution at relatively long return period ($T \gg 1$) can be written as [refer to, e.g., Abild (1994); Larsén and Mann (2009)]

$$U_T = -\alpha^{-1} \ln\left(T/(T-1)\right) + \beta, \tag{4}$$

Here T = 50 years, and this is the Annual Maximum Method (AMM). α and β are obtained through the probability-weighted moment procedure (Hosking et al., 1985; Abild, 1994):

$$\alpha = \frac{\ln 2}{2b_1 - \overline{U^{max}}}, \quad \beta = \overline{U^{max}} - \frac{\gamma_E}{\alpha}, \tag{5}$$

where $\overline{U^{max}}$ is the mean of U_i^{max}, $\gamma_E \approx 0.577215665$ is Euler's constant, and b_1 is calculated from

$$b_1 = \frac{1}{n}\sum_{i=1}^{n} \frac{i-1}{n-1} U_i^{max}. \tag{6}$$

The effect of using different length of time series on the calculation of U_{50} was extensively investigated in Larsén et al. (2015). The standard error of the Gumbel fitting is proportional to $\sqrt{1/n}$. Thus using 30-year data gives very close estimate of U_{50} to using 40 or 50-year data.

2.4 FINO masts measurements

We use the results of U_{50} at about 100 m from the three FINO masts (FINO1, FINO2 and FINO3) from Larsén et al. (2019) to compare with the calculation obtained from the three above mentioned reanalysis data and CMIP6 of his-Period. The location of the stations, the data period and length and the exact height of the data used are shown in Table 2. Their locations are also marked in Figure 2. The corresponding values of U_{50} from Larsén et al. (2019) using AMM are also listed.

2.5 Statistical significance

When using climate model output, it is always a challenge to quantify or qualify the systematic signals and uncertainties. In climate studies, the p–value analysis is often taken to address the representativeness of sample statistics in relation to the "true" or observed ones. The sample size and variability of the studied variables are two major factors affecting the degree of representativeness. However, it is not known if an ensemble of all the CMIP6 models can satisfactorily represent the historical and future climate. We can only use about one third of all CMIP6 models, namely, 18 due to data availability. This certainly increases its uncertainty. It also limits the current study to find out what these 18 models suggest about the effect of climate change on the extreme winds. It is however still relevant to ask if the change as projected by the 18 samples is significant, in comparison with the model and inter-model variability. If the change is systematic, even though the magnitude is small in relation to the spread of the sample values, or the standard deviation, it should not be ignored or considered as noise. The question is how big the magnitude of the change should be, when it is "statistically significant." Naturally, the value can be different when addressing different variables. Here, we are mostly interested in the type of turbine necessary for a given site and its possible change due to the effect of climate change.

Following the IEC standard, turbine classes I, II, III and TC (for most severe storms such as tropical cyclones) are defined based on the threshold 10-min values of U_{50} at hub height; the IEC turbine classes with corresponding extreme wind ranges are shown in Table 3. To quantify the climate change impact on the possible change in turbine class, we assign TCL = 1–4 to the four classes as in the IEC standard plus an additional class, TCL = 5, for U_{50} > 57 m s^{-1}. Note that the change of U_{50} from one class to a neighbouring class is about 7 m s^{-1}. If we use the highest class as reference, a change in U_{50} of 5% is about half of that value, suggesting a significant impact. We thus define a relative change larger than 5%

10.3389/fenrg.2024.1404791

TABLE 2 Sites and their coordinates, data period and coverage and the height where data are analyzed.

Site	Coordinates	Period	Data length (years)	Height (m)	U_{50} AMM (m s^{-1})
FINO1	6.588°E, 54.014°N	2004–2017	14	100	41.1
FINO2	13.1542°E, 55.007°N	2008–2017	10	102	35.3
FINO3	7.1583°E, 55.195°N	2010–2017	8	100	40.2

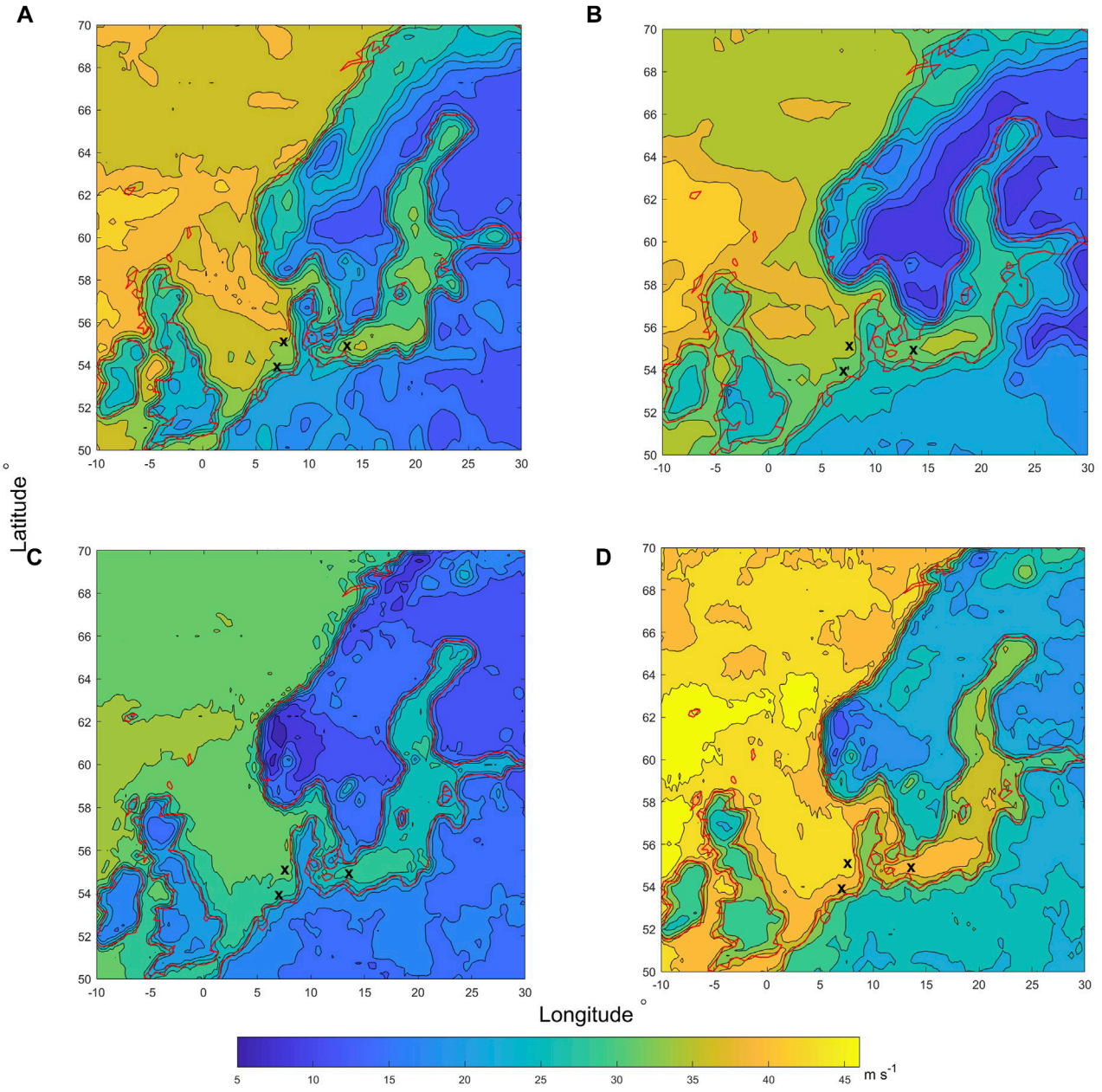

FIGURE 2
Spatial distribution of the spectral corrected 50-year wind (U_{50}) for the his-Period derived from: **(A)** CFSR data at 10 m; **(B)** MERRA2 data at 10 m; **(C)** ERA5 data at 10 m; **(D)** ERA5 data at 100 m. The positions of the three FINO masts (see Table 2) are marked with 'x'. The red lines show the coastlines.

TABLE 3 Turbine classes (TCL) with corresponding extreme wind ranges, and the assigned index.

IEC turbine class	U_{50} range, m s^{-1}	TCL
I	(0, 37.5]	1
II	(37.5, 42.5]	2
III	(42.5, 50]	3
TC	(50, 57]	4
	(57, ∞)	5

as being "significant," 2%–5% as being medium important, and less than 2% as being trivial. Note that here the word "significant" is not the same as that used in, e.g., the IPCC reports.

We compute the difference between the fut-Period and the his-Period using Equations 7-10. The difference of U_{50} between the fut-Period ($U_{50,\mathrm{fut}}$) and the his-Period ($U_{50,\mathrm{hits}}$) for each model is:

$$\Delta U_{50,\mathrm{i}} = U_{50,\mathrm{i,fut}} - U_{50,\mathrm{i,his}}, \tag{7}$$

with $i = 1, \ldots, n$, and $n = 18$. The absolute mean difference is calculated as the mean of the differences of U_{50} between the historic and future periods for the 18 models:

$$< \Delta U_{50} >= \frac{1}{n}\sum_{i=1}^{n} \Delta U_{50,\mathrm{i}}. \tag{8}$$

The relative difference is defined as

$$r_{\mathrm{U50,i}} = \left(U_{50,\mathrm{i,fut}} - U_{50,\mathrm{i,his}}\right)/U_{50,\mathrm{i,his}}. \tag{9}$$

and mean relative difference is

$$< r_{\mathrm{U50}} >= \frac{1}{n}\sum_{i=1}^{n} r_{\mathrm{U50,i}}. \tag{10}$$

A similar calculation for the second variable Q_{95} is done to obtain the absolute and relative difference ΔQ_{95} and r_{Q95}. Five ranges of r (r_{U50} and r_{Q95}) are used to quantify the change:

$$\begin{aligned} r &> 5\% \quad (SI) \\ 2\% < r &\le 5\% \quad (MI) \\ -2\% < r &\le 2\% \quad (neutral) \\ -5\% < r &\le -2\% \quad (MD) \\ r &\le -5\% \quad (SD) \end{aligned} \tag{11}$$

where SI is for significant increase, MI is for medium increase, neutral is for no obvious change, MD is for medium decrease and SD is for significant decrease.

A probability distribution of r from different models is obtained for U_{50} and Q_{95} for each grid point, to study how systematic the results are. For each grid point, we calculate the corresponding distribution values, including the mean, median, minimum, maximum and standard deviation of the distribution. We also calculate the percentage of area that suggests the five significant ranges SI, MI, neutral, MD, SD. To address if the change is significantly "systematic" at a given point, we examine if there is a 80% or more agreement of models in the sign of the change.

To roughly assess how much of the changes in U_{50} are caused by climate variability, we examine the trend in the annual wind maxima in the historic period $U_{max,i}$, with $i = 1, n$ and n the number of years of the period. The examination is done by applying a linear regression to $U_{max,i}$:

$$y = c \cdot U_{max,i} + d, \tag{12}$$

where c and d are regression coefficients, with the slope of the regression line c representing the trend, and d is less relevant. If there is a positive trend in the series of $U_{max,i}$ from the historic period, $c > 0$ and we would expect the samples of annual wind maxima to be of larger values in the future under similar variability, and therefore larger U_{50} for the future period. Thus, we expect a considerable positive correlation between c and ΔU_{50}, and vise versa for the negative correlation.

To help qualifying the CMIP6 model reliability, we compare the estimate of U_{50} from his-Period to that from the reanalysis data in Section 3.1.1. The assessment of the effect of climate change by straightforwardly comparing the results from the his-Period and fut-Period thus excludes the bias correction in the climate data. We have made this decision based on the following considerations. First, as will be shown by the results in Section 3.1.1, it is challenging to define a reference data for quantifying the bias in the climate data from either measurements or reanalysis data; the three reanalysis data show a variety of results of U_{50}. Second, it is uncertain to assume that the bias in the his-Period is the same as that in the fut-Period. To this, the only option is to make assumptions and we hereby assume that the bias is consistent in the two periods.

To further assess the robustness of the results from the 18 models, we also use sub-samples from the 18 models depending on several performance indices as presented in Section 3.1.2, thus forming two additional selections of models. The statistics are compared with those from the 18 models.

3 Results

For each model grid point, U_{50} are calculated from the reanalysis data. Both U_{50} and Q_{95} are calculated from the CMIP6 data for the his-Period and fut-Period. The results for U_{50} from the reanalysis data and CMIP6 of his-Period are presented in Section 3.1.1 and Section 3.1.2, where the quality of the CMIP6 ensemble members is discussed. The climate change impact on the extreme wind is analyzed in Section 3.2.

3.1 Extreme wind in the historic period

3.1.1 Reanalysis data

The 50-year wind U_{50} at 10 m from the CFSR, MERRA2 and ERA5 reanalysis data are shown in Figure 2 for the his-Period. Over water, the spatial gradient in U_{50} is similar in the three data sets, with the highest values northwest of the British Islands and lowest in the northern Baltic Sea. Among the three, the CFSR and MERRA2-derived U_{50} are more similar with respect to the spatial patterns and

magnitudes. The ERA5 U_{50} at 10 m is, on average, systematically smaller. Over land, an obvious difference between ERA5 and the other two reanalysis data is the distribution over Norway and Sweden, where both CFSR and MERRA2 data suggest stronger extreme wind over western Norway and the smallest at approximate 61°N over Sweden, while the ERA5 data suggest lower extreme wind over western Norway and the smallest on the west coast at ~61°N. These patterns are suggested to be related to extremely high surface roughness lengths in MERRA2 over forest and the use of orographic drag in the ERA5 model (Dörenkämper et al., 2020). The spatial distribution is similar for the ERA5 data at 10 m and 100 m.

As mentioned in Section 1, a global atlas of U_{50} was made available in the GASP project at a spatial grid spacing of 275 m. We compare the spatial distribution of U_{50} at 100 m from ERA5 (Figure 2D) and U_{50} at 100 m from the GASP project (see Figure 5 in Larsén et al. (2022)). In the GASP data, the values of U_{50} at 100 m over water were derived using those at 10 m assuming a logarithmic wind profile and a surface roughness length parameterization from the Simulating WAves Nearshore (SWAN) model (Larsén et al., 2022); over land, the values from the CFSR reanalysis data were downscaled using microscale modeling; see also Larsén et al. (2022). The large scale pattern of U_{50} from GASP is consistent with what we observed here in Figure 2. The values of U_{50} at 100 m over land vary by 20–40 m s^{-1} and those over water from about 25 to 55 m s^{-1}. Offshore, these values are of comparable magnitude to those in Figure 2D, namely, ERA5 data at 100 m.

Due to the differences in the various reanalysis data it is difficult to decide which one of them is the best without a systematic validation with measurements. But a global database of such measurements does not exist. Thus, we focus on the characteristics of the wind distribution that are shared by these reanalysis data and use them to discuss the quality of the CMIP6 data for his-Period. We use the following wind characteristics that are present in the three reanalyses as basic quality check for the CMIP6 data: (a) A 50-year wind at 100 m $U_{50,100m}$ that ranges between about 5 and 55 m s^{-1} over the domain; (b) Stronger extreme winds over the North Sea than over the Baltic Sea; (c) Strongest U_{50} in the northern North Sea; (d) Clear land-sea difference with stronger winds over water. We use these four characteristics to create an index, defined as the large-scale score (with 0 meaning "not matching" and 1 meaning "matching"), and use it for data analysis of the CMIP6 model outputs (Table 4).

3.1.2 CMIP6 data

We use the same procedure as used for the reanalysis data, e.g., through the spectral correction method, Annual Maximum Method and the Gumbel distribution fit, to calculate U_{50} for the 18 CMIP6 models at three heights 50, 100, and 200 m. The height of 100 m is shown in Figure 3 from the 18 CMIP6 models.

We use the four characteristics, (a)–(d), as described at the end of Section 3.1.1 to give a score 0 or 1 to the 18 models. The results of this scoring are summarized in Table 4. The four criteria are generous, and therefore the scoring is qualitative; all models satisfy the basic quality criteria (a) and (b). In the end, we have 6 models with highest score 4 (models 1, 5, 6, 9, 10, 18) and 3 models with lowest score 2 (models 8, 11, 14). As introduced in Section 2.5, to explore the sensitivity of results to the collection of model data, in addition to the analysis using all 18 models (called "All-group"), we also perform the data analysis using two sub-groups of models: "Score-4-group" (including all models of a score of 4: 6 models), and "Score-3/4-group" (including models with a score of 3 or 4: 15 models). The model grouping is also shown in Table 4.

We validate the calculations of U_{50} at 100 m from the CMIP6 data with those from measurements at the three FINO masts from Larsén et al. (2019) (Table 2). Note that the data periods and lengths from the FINO sites are shorter and different from the CMIP6 historical data; this can bring uncertainties to the comparison. As mentioned in Section 2.2, for CFSR and MERRA2 data, due to the uncertainties in calculating wind speeds at 100 m from wind speeds from 10 m or 50 m, we avoid examining the wind speeds at 100 m over the entire domain. For the water sites FINO 1, 2, and 3, we used the same method as in the GASP project (section 2.2; Larsén et al. (2022)) to extrapolate the winds of CFSR and MERRA2 data to 100 m, in order to compare with the measurements. Figure 4 presents the difference of the estimates of U_{50} in percentage between the measured and modeled values for the three FINO sites. Even though some CMIP6 models provide more consistent large scale patterns, their performance at the three offshore sites are not necessarily best (e.g., model 10). Models with lowest large-scale scores as in Table 4 (model 11 and 14) also show poor performance at the three sites, while the performance of model 8, which as a large-scale score of 2, has little bias.

3.2 Climate change impact on the extreme wind

The effect of climate change on the extreme wind is estimated through parameters defined in Section 2.5. This includes the mean and relative differences in U_{50} and Q_{95} from the 18 models at each grid point (Figures 5, 6). A description of the model spread of the differences at each grid point is shown in Figure 7 and the summary statistics over the entire domain are shown in Table 5.

We first explore the effect of climate change on U_{50} and Q_{95}. For each grid point, a distribution of the five kinds of change (SI, MI, neutral, MD, SD) with the corresponding number of supportive models is made (not shown). The change corresponding to the largest number of supportive models is extracted and shown in Figure 7 for each grid point. This is done to the All-group (a,b), Score-4-group (c,d) and Score-3/4-group (e,f), and the results are shown as the three rows in this figure, respectively. The left column is for U_{50}, and the right column is for Q_{95}.

Figures 5, 6 show high consistency of the spatial patterns of ΔU_{50} and ΔQ_{95}. At first glance, the CMIP6 models prediction for the future suggest an increase in the extreme wind over the west part of the domain (including the United Kingdom, Denmark and parts of Germany) and a decrease in the northwestern Atlantic. The results also indicate that climate change could lead to reduced extreme wind over most of the eastern part of the model domain, including Sweden, Finland, parts of Poland and middle part of the Baltic Sea for the near future (2020–2049) based on the SSP585 high emission scenario. These features are present in All-group, Score-4-group and Score-3/4-group. When being averaged over the entire domain with all models included, the future U_{50} is 0.2 m s^{-1} weaker than the historic value with a standard deviation 0.5 m s^{-1} among the 18 models. The corresponding minimum, median and maximum

TABLE 4 Score of the large-scale extreme wind for the his-Period for the 18 CMIP6 models (labeled as defined in Table 1) using the four wind characteristics defined in Section 3.1.2. Also shown are the three model groups. The third column "corr" is the correlation between c the regression slope coefficient in Equation 12 ($U_{max,i}$) and ΔU_{50} for each model at all grid points.

No.	Model	Corr	a	b	c	d	Total	All-group	Score-4-group	Score-3/4-group
1	ACCESS-CM2	−0.26	1	1	1	1	4	*	*	*
2	CanESM5	−0.18	1	1	1	0	3	*		*
3	CESM2	−0.19	1	1	1	0	3	*		*
4	CMCC-CM2-SR5	0.23	1	1	1	0	3	*		*
5	CNRM-CM6-1	−0.35	1	1	1	1	4	*	*	*
6	CNRM-ESM2-1	−0.09	1	1	1	1	4	*	*	*
7	HadGEM3-GC31-LL	0.33	1	1	1	0	3	*		*
8	HadGEM3-GC31-MM	0.42	1	1	0	0	2	*		
9	IPSL-CM6A-LR	−0.19	1	1	1	1	4	*	*	*
10	MIROC6	−0.08	1	1	1	1	4	*	*	*
11	MIROC-ES2L	0.07	1	1	0	0	2	*		
12	MPI-ESM1-2-HR	−0.05	1	1	1	0	3	*		*
13	MPI-ESM1-2-LR	−0.21	1	1	1	0	3	*		*
14	MRI-ESM2-0	0.18	1	1	0	0	2	*		
15	NESM3	0.23	1	1	1	0	3	*		*
16	NorESM2-LM	−0.03	1	1	1	0	3	*		*
17	NorESM2-MM	0.16	1	1	1	0	3	*		*
18	UKESM1-0-LL	0.22	1	1	1	1	4	*	*	*

value of ΔU_{50} is −1.7, −0.2 and 1.1 m s^{-1}, suggesting an overall weaker extreme wind. However, these values are rather small and less than 2%.

Table 5 summarizes the statistics for the three groupings. The All-group is rather similar to the Score-3/4-group, while the Score-4-group, which has only 6 models, shows slightly larger differences but consistent results. For the majority of grid points in the model domain, most models indicate no obvious change ("neutral" ~35 – 52% of grid points depending on the ensemble group), and many grid points show significant increase or significant decrease. From Figure 7, the CMIP6 models suggest the largest chance of reduced extreme winds in the near future mostly over land in the middle part of Norway and Sweden and part of Poland. Over the Baltic Sea, the CMIP6 ensemble suggests the largest possibility of reduced extreme wind in the north, but of increased extreme wind in the south. For all 5 ranges of r in Equation 11, there are no grid points where 80% or more of the models suggest the same trend. However, when combining the last two ranges of r, namely, $r < 0$, there are a few grid points where 80% or more of the All-group suggest the same conclusion; these grid points are marked with "x" in Figure 7A for U_{50} and b for Q_{95}.

The correlation coefficient between c as in Equation 12 and ΔU_{50} for each model is provided in Table 4 (column 3). For all models, all grid points, the overall average correlation coefficient is 0.03, almost zero. None of the models suggests a considerable positive dependence of the change in U_{50} on the linear trend from the historic period (c). This implies an overall weak impact from the climate variability on the change in U_{50}. We therefore attribute the change to climate change, rather than the climate variability.

To discuss the relevance and importance of the climate change effect on the extreme winds, we relate the extreme wind change to the turbine class as defined in the IEC standard (IEC, 2019) (Table 3). The corresponding changes in turbine class are calculated for each CMIP6 model and each grid point. When requiring the level of statistical significance for climate studies, 80% of the samples, be consistent in the signals, all grid points suggest no TCL-change. It is still so when lowering the level from 80% to 50%. Behind this conclusion lies the fact that individual models indicate locations with TCL-change rather differently, and therefore do not conform to statistical significance for TCL-change. Here we use the Score-4-group as an example; the TCL-change at

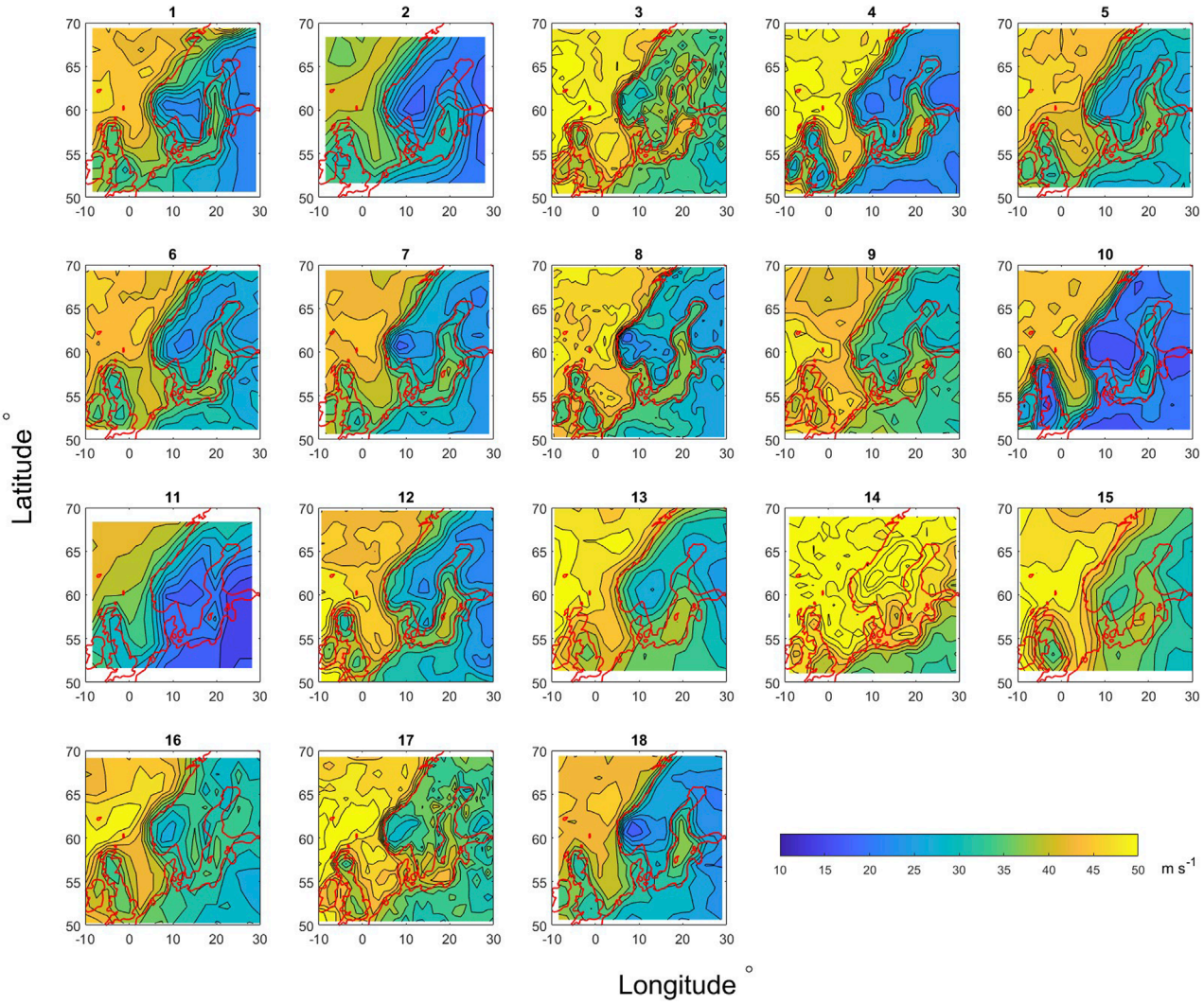

FIGURE 3
The 50-year wind at 100 m for the 18 CMIP6 models for the his-period, $U_{50,his}$, estimated using the spectral correction method. The model's labels follow those defined in Table 1. The red lines show the coastlines.

100 m in the six models are shown in Figure 8. For each grid point, the majority of the models suggest no TCL-change, but each model has its own locations for the red (stronger TCL) and blue (weaker TCL) boxes. For instance, model 1 (Figure 8A) suggests a lower turbine class in the near future over the water in the north, and a higher turbine class in part of the southern North Sea; model 9 (Figure 8D) has contradicting suggestions. Model 5 (Figure 8B) suggests higher TCL in the coast areas of Norway, Finland, Denmark, the Baltic Sea and south of the North Sea, to which model 18 (Figure 8F) has contradicting suggestions (except for the most northern part of the United Kingdom). These results suggest that in this region there is no conclusive trend in the change in the extreme winds that will provoke a shift towards the need for higher TCL in the future. A change towards a higher TCL would make wind energy development more expensive. The same analysis was performed at 50 and 200 m; the conclusions are the same as at 100 m.

4 Discussion

We investigated the climate change effect on the 50-year wind, which is one of the key design parameters for wind turbines. We used outputs from 18 CMIP6 models, which is about one third of all models submitted to CMIP6. We also chose to use the high-emission SSP585 scenario, following Hahmann et al. (2022). Such a selection faces the question whether this collection of models is sufficient for drawing robust conclusions. The models were chosen because of the availability of a number of variables needed for deriving the wind speeds at turbine hub heights from the values at model levels (Hahmann et al., 2022). In addition, in terms of wind resources, Hahmann et al. (2022) showed good agreement with observations for the historical period for the North Sea for at least 16 of the 18 models. This is however not directly transferable to extreme winds. With this limitation, we note that the analysis and conclusions drawn here may be updated in the future when

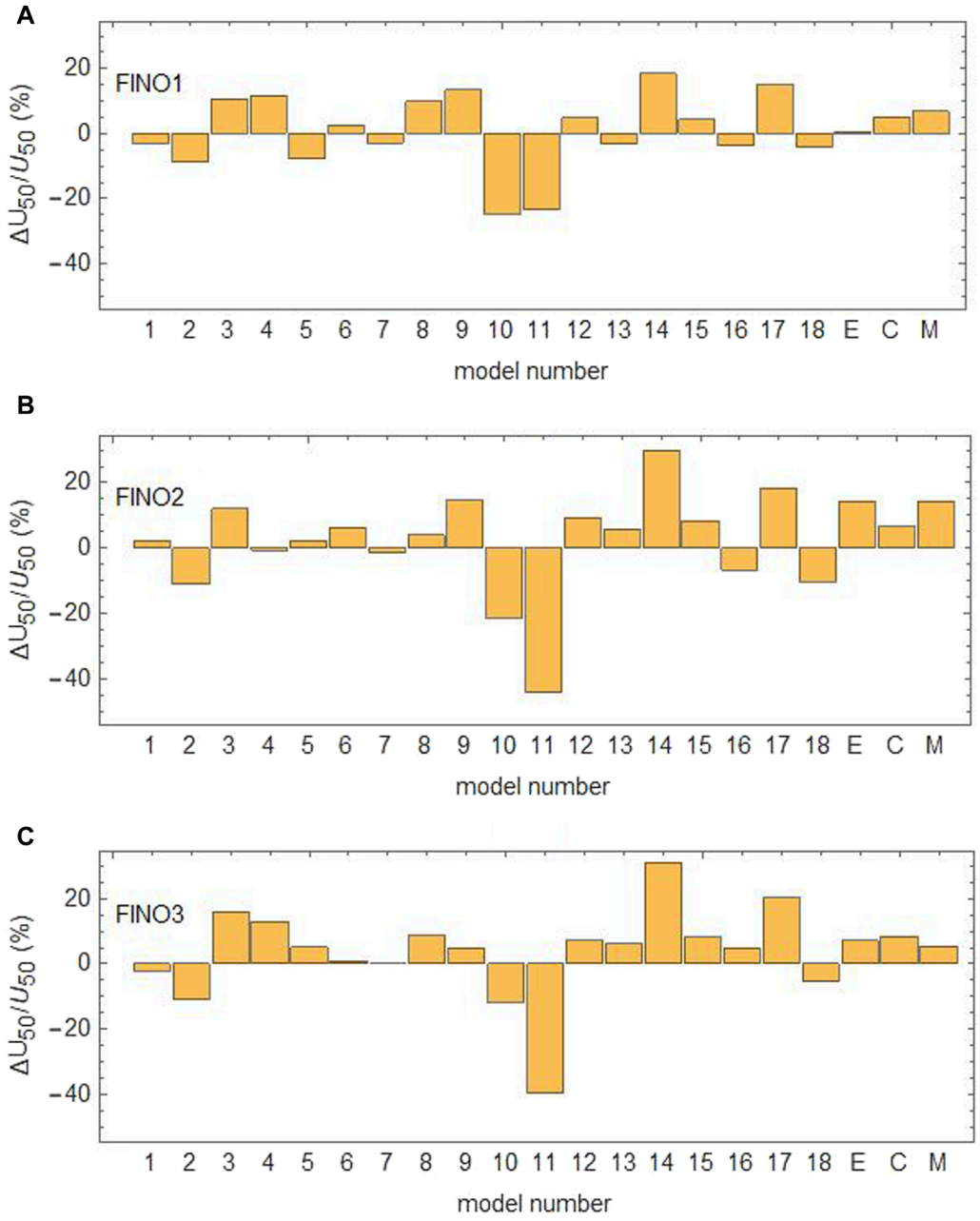

FIGURE 4
Comparison of U_{50} at 100 m at the three measurement sites: **(A)** FINO1, **(B)** FINO2 and **(C)** FINO3, between the observed value and that of the 18 CMIP6 models (labeled as defined in Table 1) for the his-Period, as well as that of the three reanalysis data, with 'E' for ERA5, 'C' for CFSR1 and 'M' for MERRA2. The values are $\Delta U_{50}/U_{50,obs}$, where $\Delta U_{50} = U_{50,obs} - U_{50,CMIP6}$, with $U_{50,obs}$ from Larsén et al. (2019).

more relevant data are made available by the community. At the same time, it is worth finding out what the 18 models suggest regarding the climate change effect on the extreme wind and more relevantly to wind energy application, the change in the choice of turbine class.

A common challenge in analyzing ensemble data is to separate the "signal" from the "noise," as signals can be buried in the group of models (e.g., Outten and Esau, 2013; Smith et al., 2020). Smith et al. (2020) pointed it out: "Quantifying signals and uncertainties in climate models is essential for the detection, attribution, prediction and projection of climate change." Even within different reanalysis products that should be representative of the historic data, there are already significant discrepancies in their estimations of extreme winds, here, particularly over land. The measurements used here are from three offshore sites, thus evaluation based on the FINO locations would strongly underrate both the model scatter and wind extreme changes over the region as the whole. Our approach for "extracting signals" of the effect of climate change include the comparison of the large scale distribution pattern of the extreme wind between the CMIP6 model data that are consistently presented

10.3389/fenrg.2024.1404791

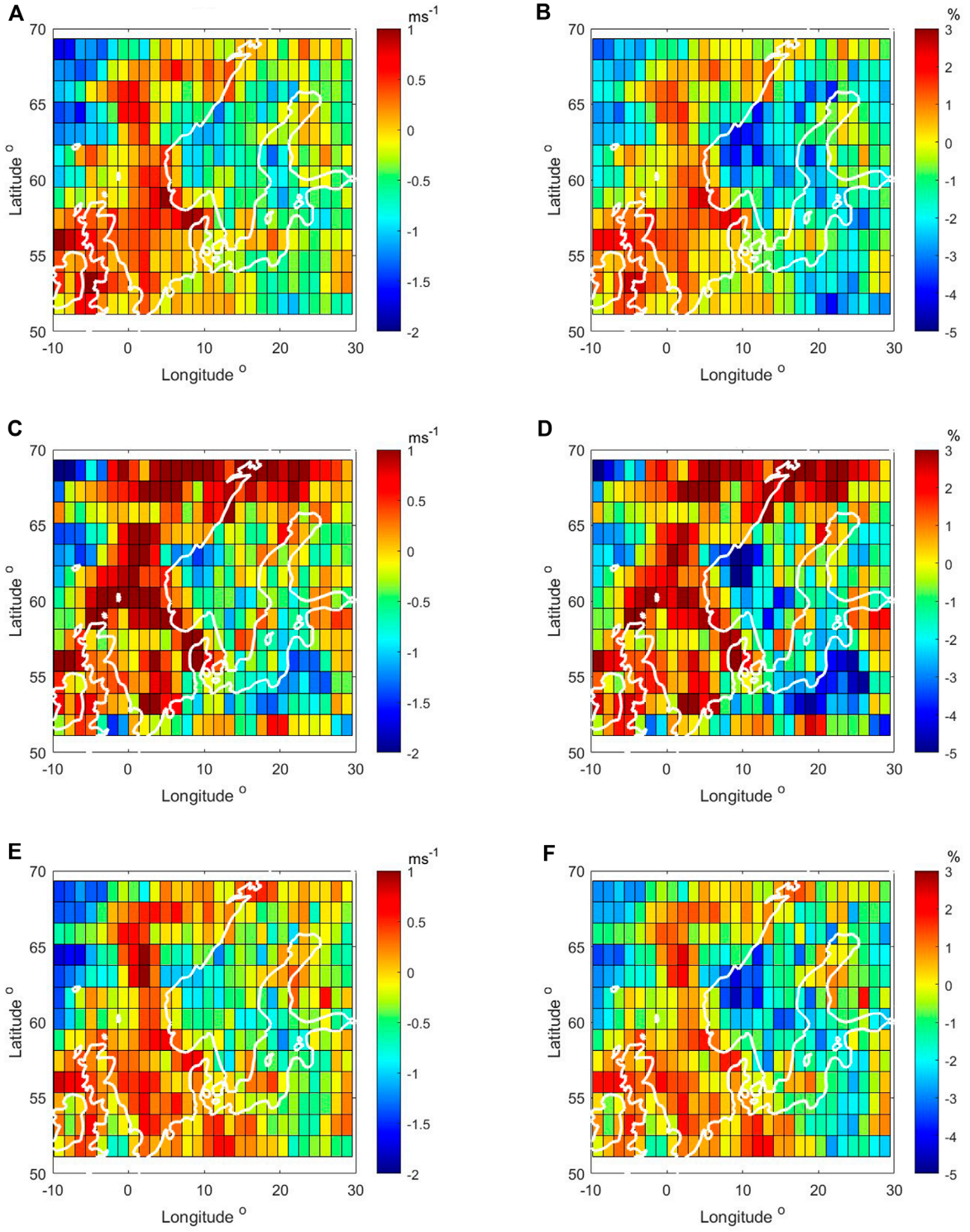

FIGURE 5
Spatial distribution of model mean difference ΔU_{50} (left column) and relative mean difference ($\Delta U_{50}/U_{50,his}$, right column) between the his- and fut-Periods. for model All-group **(A, B)**, Score-4-group **(C, D)**; and Score-3/4-group **(E, F)**.

by the three reanalysis data, and the average of the increase and decrease in the extreme wind parameters in the model ensemble. It must be noted that the chosen analysis approach is based on the assumption that consistent behaviour between the CMIP6 models is an indicator for higher probability of occurrence under the given scenario (e.g., Christensen et al., 2019). This assumption is commonly used in the IPCC assessment report (IPCC, 2021). There are systematic and consistent patterns for increased and decreased

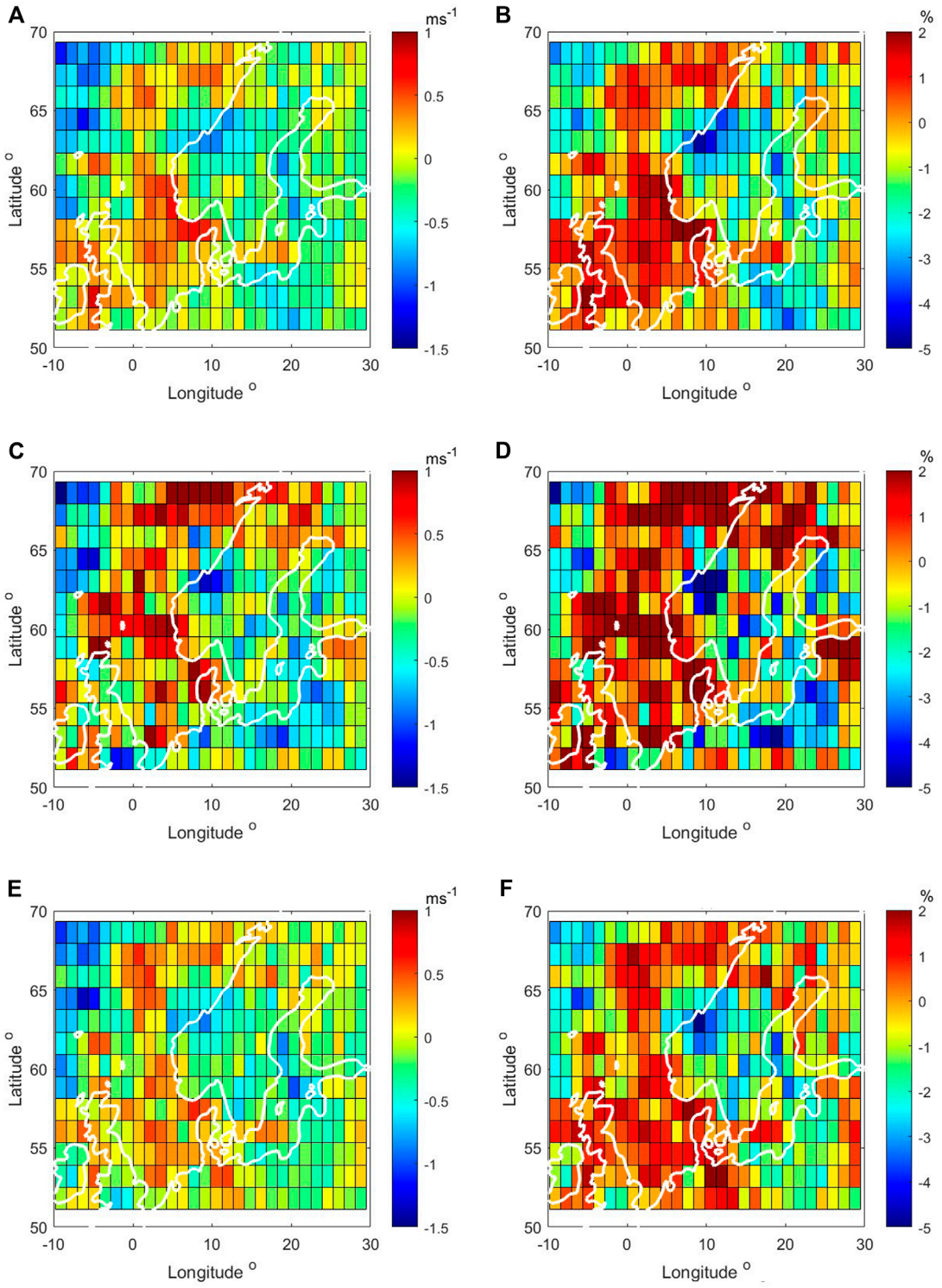

FIGURE 6
Same as Figure 5, but for the 95% quantile of the wind speed at 100 m. For model All-group **(A, B)**, Score-4-group **(C, D)** and Score-3/4-group **(E, F)**.

extreme winds that can be identified in certain regions, for both U_{50} and Q_{95}. We used three different groups, with one including 18 models, one with 6 models and one with 15 models, depending on several performance indices, in order to get a qualitative assessment of how sensitive the results are to the models.

Among the many studies on climate change impact, the impact on extreme wind conditions does not lead to a clear conclusion. The following patterns have been identified in earlier studies using different model outputs and scenarios: (a) Overall increasing extreme wind parameters in Northern Europe (e.g., Donat et al.,

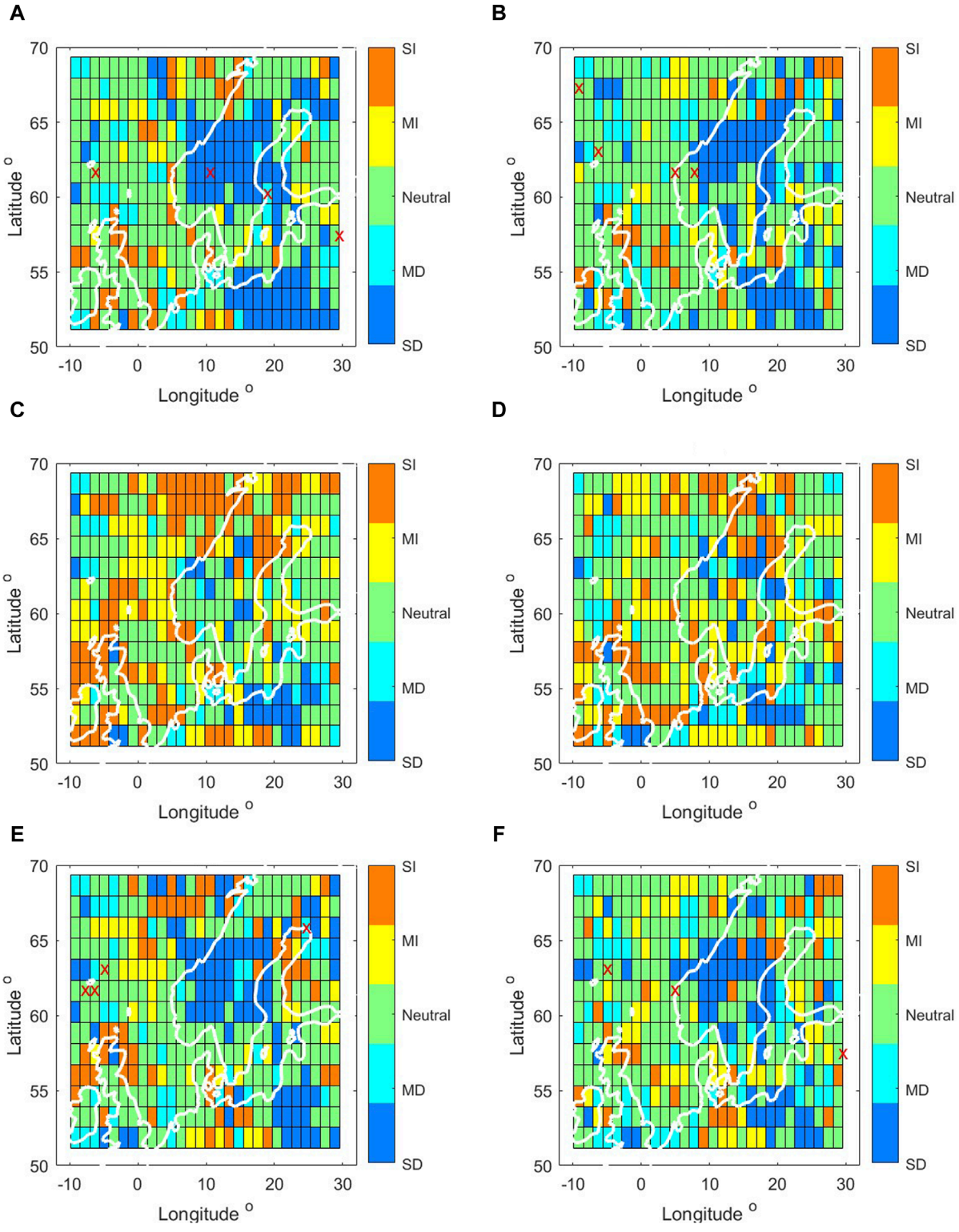

FIGURE 7
Range (SI–significant increase, MI–medium increase, neutral–no obvious change, MD–medium decrease, SD–significant decrease, see text) in relative change in ΔU_{50} (left column) and ΔQ_{95} (right column) at 100 m supported by the largest number of CMIP6 models in All-group **(A, B)**, Score-4-group **(C, D)**, and Score-3/4-group **(E, F)**. Red crosses in **(A)** and **(B)** mark the grid points where 80% or more of the All-group suggest consistently $r < 0$.

10.3389/fenrg.2024.1404791

TABLE 5 Summary of the statistics of change in the extreme wind ΔU_{50} at 100 m (Figure 5) and ΔQ_{95} (Figure 6) over the entire domain.

Variables	Statistics	Grouping of CMIP6 models		
		All-group	Score-4-group	Score-3/4-group
		(all models)	(models 1, 5, 6, 9, 10, 18)	(models 1–7, 9, 10, 12, 13, 15–18)
$r_{U_{50}}$	SI area (%)	24.4	8.4	20.7
	MI area (%)	12.6	8.4	12.3
	neutral area (%)	44.1	34.7	40.9
	MD area (%)	8.1	22.2	10.6
	SD area (%)	10.8	26.4	15.5
r_{Q95}	SI area (%)	19.5	8.6	17.5
	MI area (%)	13.3	12.1	13.1
	neutral area (%)	50.0	37.7	45.8
	MD area (%)	9.4	22.0	13.8
	SD area (%)	7.9	19.7	9.9

2011; Pryor et al., 2012; Christensen et al., 2022); (b) Increase over the Baltic Sea (e.g., Nikulin et al., 2011; Christensen et al., 2022); (c) Small insignificant increase with large spread in the southern part of the Baltic Sea. Christensen et al. (2022) found from 72 EURO-CORDEX RCP8.5 simulations very little agreement even on the sign of wind speed change. With the current study, some key statistics can be summarized (see, e.g., Table 5), including: about 40% of domain area corresponds to no considerable change, 20% corresponds to significant increase and a slightly smaller area suggests significant decrease. Geographically, quite a large area of the North Sea corresponds to an average increase, and most part of the Baltic Sea and the Scandinavian Peninsula corresponds to an average decrease. Most analyses here also support a medium increase in southern part of the Baltic Sea. While the analysis has also shown some degree of sensitivity regarding the models used, the overall conclusions are consistent (Figures 5–7). For all five ranges of r, there is no single grid point where 80% or more of the models suggest the same change. However, there are 4 or less grid points over the entire domain, as marked in Figure 7 for the relatively larger groups All-group and Score-3/4-group, where more than 80% of the model suggest $r < 0$. It is however difficult to draw further conclusions from the very few grid points.

It should be noted that here for both his-Period and fut-Period, 30-year long data are used in connection with Equations 4–6. Data length of 30-year is considered a sufficient length for the calculation of 50-year return wind for the studied area (e.g., Larsén et al., 2015). However, if an extreme wind event has a return period longer than 30-year, it could not be detected in our calculations.

We assess the importance of the effects of climate change on the extreme wind (and thus on wind turbine siting), by relating the results to the IEC standards and discuss how it affects the design criteria for turbines. There is a high diversity between models on the general analysis of extreme wind and there is no consensus anywhere in the studied domain regarding if it will be more expensive or cheaper in the future to install wind turbines (Figure 8). Most models suggest no change in turbine class over most grid points in the study area. Using different reference model grids and interpolation methods to convert different model data to common grid points do not change the conclusion. It is expected that a high resolution regional modeling downscaled from the CMIP6 data will bring much more spatial variability. The corresponding regional model output will be valuable for updating the analysis in this study. Such a downscaling to a spatial resolution of a few kilometers is a big project and it will take the community some time to accomplish. However, these regional modeling is often done with historical land use classes, which limits its usefulness to wind-related studies. This study only downscales the CMIP6 data in temporal domain using the spectral correction method, so that the calculated extreme wind of the time series matches that of a 10-min time series (requirement from the IEC standard). The spatial details, however, are thus not resolved. For the 18 CMIP6 models, the quality of the extreme wind simulation, which is assessed through the comparison of extreme wind distribution pattern with reanalysis data and comparison with values from measurements at three offshore sites, did not suggest that higher resolution gives better agreement with measurements. This is likely because the spatial resolution of all of these model data are too coarse and all the sites are offshore. These data have a spatial resolution ranging from about 80 km to a couple of hundreds of kilometers. This will of course introduce uncertainties and thus we can only discuss the effect of climate change on a large scale.

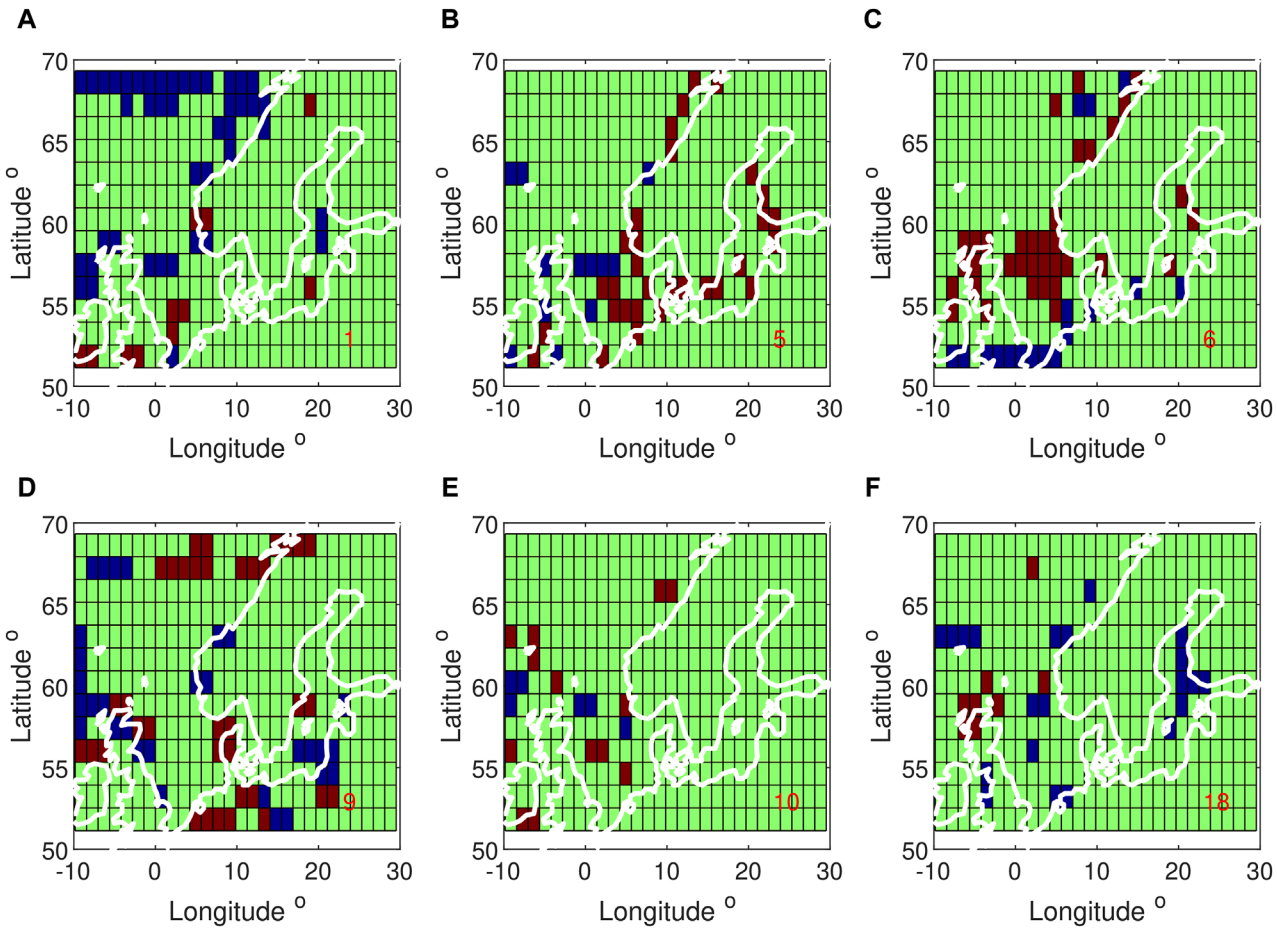

FIGURE 8
Change in the future TCL for 100 m in the six models in Score-4-group: **(A)** model 1: ACCESS-CM2; **(B)** model 5: CNRM-CM6-1; **(C)** model 6: CNRM-ESM2-1; **(D)** model 9: IPSL-CM6A-LR; **(E)** model 10: MIROC6; **(F)** model 18: UKESM1-0-LL. The colors indicate: one class stronger (red), one class weaker (blue) and no changes (green).

5 Conclusion

Eighteen CMIP6 ensemble members are used to assess climate change impact on extreme wind over Northern Europe. There is a large diversity of suggestions of impacts between the model members. The analysis shows an overall increase in the extreme winds in the North Sea and southern part of the Baltic Sea, but a decrease in the Scandinavian Peninsula and most part of the Baltic Sea. However, the wind climate change as projected by the CMIP6 SSP585 models does not suggest more expensive or cheaper turbines will need to be installed in the area.

Data availability statement

The datasets presented in this study can be found in online repositories. The names of the repository/repositories and accession number(s) can be found in the article/Supplementary Material.

Author contributions

XL: Conceptualization, Data curation, Formal Analysis, Funding acquisition, Methodology, Resources, Writing–original draft, Writing–review and editing. MI: Data curation, Formal Analysis, Investigation, Validation, Writing–review and editing. ÁH: Data curation, Formal Analysis, Writing–review and editing.

Funding

The author(s) declare that financial support was received for the research, authorship, and/or publication of this article. This study is supported by the GASPOC project (EUDP 64020-1043) and EU Horizon project DTWO (HE 101146689).

Acknowledgments

The ERA5 data were downloaded from ECWMF and Copernicus climate change Service Climate Data Store. MERRA2

data are downloaded from the Distributed Active Archive Center (GSFC DAAC), https://doi.org/10.5067/VJAFPLI1CSIV. FINO 1, 2, and 3 were supplied by German Federal Maritime And Hydrographic Agency (BSH). CFSR data have been retrieved from the Research Data Archive of the National Center for Atmospheric Research (https://doi.org/10.5065/D6513W89). The CMIP6 multi-model ensemble data were downloaded through the distributed data archive developed and operated by the Earth System Grid Federation (ESGF; https://esgf.llnl.gov/). We thank our colleague Andrea Hahmann for advice and comments, and for preparing the CMIP6 data.

Conflict of interest

The authors declare that the research was conducted in the absence of any commercial or financial relationships that could be construed as a potential conflict of interest.

Publisher's note

Supplementary material

The Supplementary Material for this article can be found online at: https://www.frontiersin.org/articles/10.3389/fenrg.2024.1404791/full#supplementary-material

References

Abild, J. (1994). Application of the wind atlas method to extremes of wind climatology. *Forskningscenter Risoe*. Risoe-R-722(EN).

Bastine, D., Larsén, X., Witha, B., Dörenkämper, M., and Gotschall, J. (2018). Extreme winds in the new european wind atlas. *J. Phys. Conf. Ser.* 1102, 012006. doi:10.1088/1742-6596/1102/1/012006

Beniston, M., Stephenson, D. B., Christensen, O. B., Ferro, C. A. T., Frei, C., Goyette, S., et al. (2007). Future extreme events in european climate: an exploration of regional climate model projections. *Clim. Change* 81, 71–95. doi:10.1007/s10584-006-9226-z

Boucher, O., Servonnat, J., Albright, A. L., Aumont, O., Balkanski, Y., Bastrikov, V., et al. (2020). Presentation and evaluation of the IPSL-CM6A-LR climate model. *J. Adv. Model. Earth Syst.* 12, e2019MS002010. doi:10.1029/2019MS002010

Brasseur, G., and Carlson, D. (2015). Future directions for the world climate research programme. *EOS* 96. doi:10.1029/2015EO033577

Cherchi, A., Fogli, P. G., Lovato, T., Peano, D., Iovino, D., Gualdi, S., et al. (2019). Global mean climate and main patterns of variability in the CMCC-CM2 coupled model. *J. Adv. Model. Earth Syst.* 11, 185–209. doi:10.1029/2018MS001369

Christensen, J., Larsen, M., Christensen, O. e. a., Drews, M., and Stendel, M. (2019). Robustness of european climate projections from dynamical downscaling. *Clim. Dyn.* 53, 4857–4869. doi:10.1007/s00382-019-04831-z

Christensen, O. B., Kjellström, E., Dieterich, C., Gröger, M., and Meier, H. E. M. (2022). Atmospheric regional climate projections for the baltic sea region until 2100. *Earth Syst. Dyn.* 13, 133–157. doi:10.5194/esd-13-133-2022

Clausen, N.-E., Larsén, X., Pryor, S., and Drews, M. (2012). Wind power, in "*Climate Change and Energy Systems—Impacts, Risks and Adaption in the Nordic and Baltic countries*". Editors T. Thorsteinn, and B. Halldór (TemaNord: Nordic Council of Ministers), 147–160. No. 502 in TemaNord. Print: Arco Grafisk A/S.

Danabasoglu, G., Lamarque, J.-F., Bacmeister, J., Bailey, D. A., DuVivier, A. K., Edwards, J., et al. (2020). The community earth system model version 2 (cesm2). *J. Adv. Model. Earth Syst.* 12, e2019MS001916. doi:10.1029/2019MS001916

[Dataset] WCRP Working Group on Coupled Modeling (WGCM) (2004). Prediction of regional scenarios and uncertainties for defining european climate change risks and effects (prudence). Available at: https://www.wcrp-climate.org/modelling-wgcm-mip-catalogue/modelling-wgcm-mips-2/288-modelling-wgcm-catalogue-prudence (Accessed March, 2024).

Della-Marta, P., Mathis, H., Frei, C., Liniger, M., Kleinn, J., and Appenzeller, C. (2009). The return period of wind storms over europe. *Int. J. Climatol.* 29, 437–459. doi:10.1002/joc.1794

Donat, M. G., Leckebusch, G. C., Wild, S., and Ulbrich, U. (2011). Future changes in european winter storm losses and extreme wind speeds inferred from GCM and RCM multi-model simulations. *Nat. Hazards Earth Syst. Sci.* 11, 1351–1370. doi:10.5194/nhess-11-1351-2011

Dörenkämper, M., Olsen, B. T., Witha, B., Hahmann, A. N., Davis, N. N., Barcons, J., et al. (2020). The making of the new European wind atlas - Part 2: production and evaluation. *Geosci. Model Dev.* 13, 5079–5102. doi:10.5194/gmd-13-5079-2020

Eyring, V., Bony, S., Meehl, G. A., Senior, C. A., Stevens, B., Stouffer, R. J., et al. (2016). Overview of the coupled model Intercomparison project phase 6 (CMIP6) experimental design and organization. *Geosci. Model Dev.* 9, 1937–1958. doi:10.5194/gmd-9-1937-2016

Gelaro, R., McCarty, W., Suárez, M. J., Todling, R., Molod, A., Takacs, L., et al. (2017). The modern-era retrospective analysis for research and applications, version 2 (merra-2). *J. Clim.* 30, 5419–5454. doi:10.1175/jcli-d-16-0758.1

Giorgi, F., and Gutowski, W. J. (2015). Regional dynamical downscaling and the CORDEX initiative. *Annu. Rev. Environ. Resour.* 40, 467–490. doi:10.1146/annurev-environ-102014-021217

GWEC (2022). *Global wind report 2022*. Brussels, Belgium: Global Wind Energy Council

Hahmann, A. N., García-Santiago, O., and Peña, A. (2022). Current and future wind energy resources in the north sea according to CMIP6. *Wind Energy Sci.* 2022, 2373–2391. doi:10.5194/wes-7-2373-2022

Hajima, T., Watanabe, M., Yamamoto, A., Tatebe, H., Noguchi, M. A., Abe, M., et al. (2020). Development of the miroc-es2l earth system model and the evaluation of biogeochemical processes and feedbacks. *Geosci. Model Dev.* 13, 2197–2244. doi:10.5194/gmd-13-2197-2020

Hansen, B. O., Larsén, X. G., Kelly, M., Rathmann, O. S., Berg, J., Bechmann, A., et al. (2016). Extreme wind calculation applying spectral correction method—test and validation. *Tech. Rep. Wind Energy Dep*, DTU Wind Energy E-0098.

Hersbach, H., Bell, B., Berrisford, P., Hirahara, S., Horányi, A., Muñoz-Sabater, J., et al. (2020). *The ERA5 global reanalysis 146*, 1999–2049. doi:10.1002/qj.3803

Hosking, J., Wallis, J. R., and Wood, E. F. (1985). Estimation of the generalized extreme value distribution by the method of probability-weighted moments. *Technometrics* 27, 251–261. doi:10.1080/00401706.1985.10488049

IEC (2019). "IEC 61400-1 Ed4: wind turbines - Part 1: design requirements," in *standard*. Geneva, Switzerland: International Electrotechnical Commission.

Imberger, M., and Larsén, X. (2022). Sensitivity and quality assessment of the global 50-year return winds using reanalysis products and measurements. *Wind. Annu. Event.* (ilbao, Spain), April, 2022. https://windeurope.org/annual2022/

IPCC (2021). *Climate change 2021: the physical science basis. Contribution of working group I to the sixth assessment report of the intergovernmental panel on climate change*. Cambridge, United Kingdom, and New York, USA: Cambridge University Press. doi:10.1017/9781009157896.002

Kawai, H., Yukimoto, S., Koshiro, T., Oshima, N., Tanaka, T., Yoshimura, H., et al. (2019). Significant improvement of cloud representation in the global climate model mri-esm2. *Geosci. Model Dev.* 12, 2875–2897. doi:10.5194/gmd-12-2875-2019

Larsén, X., Kruger, A., Floors, R., Cavar, D., and Hahmann, A. (2021). Extreme gust atlas over South Africa. *EGU General Assem. 2021*. online, 19–30 Apr 2021, EGU21-5829. doi:10.5194/egusphere-egu21-5829

Larsén, X., and Mann, J. (2006). The effects of disjunct sampling and averaging time on maximum mean wind speeds. *J. Wind Eng. Ind. Aerodyn.* 94, 581–602. doi:10.1016/j.jweia.2006.01.020

Larsén, X., and Mann, J. (2009). Extreme winds from the NCEP/NCAR reanalysis data. *Wind Energy* 12, 556–573. doi:10.1002/we.318

Larsén, X., Mann, J., Rathmann, O., and Jørgensen, H. E. (2015). Uncertainties of the 50-year wind from short time series using generalized extreme value distribution and generalized pareto distribution. *Wind Energy* 18, 59–74. doi:10.1002/we.1683

Larsén, X. G., Davis, N., Hannesdóttir, Á., Kelly, M., Svenningsen, L., Slot, R., et al. (2022). The global atlas for siting parameters project: extreme wind, turbulence, and turbine classes. *Wind Energy* 25, 1841–1859. doi:10.1002/we.2771

Larsén, X. G., Du, J., Bolanos, R., Imberger, M., Kelly, M., Badger, M., et al. (2019). Estimation of offshore extreme wind from wind-wave coupled modeling. *Wind Energy* 22, 1043–1057. doi:10.1002/we.2339

Larsén, X. G., and Kruger, A. (2014). Application of the spectral correction method to reanalysis data in South Africa. *J. Wind Eng. Industrial Aerodynamics* 133, 110–122. doi:10.1016/j.jweia.2014.08.002

Larsén, X. G., Ott, S., Badger, J., Hahmann, A. H., and Mann, J. (2012). Recipes for correcting the impact of effective mesoscale resolution on the estimation of extreme winds. *J. Appl. Meteorology Climatol.* 51, 521–533. doi:10.1175/JAMC-D-11-090.1

Larsén, X. G., Vincent, C. L., and Larsen, S. (2013). Spectral structure of mesoscale winds over the water. *Q. J. R. Meteorological Soc.* 139, 685–700. doi:10.1002/qj.2003

Mauritsen, T., Bader, J., Becker, T., Behrens, J., Bittner, M., Brokopf, R., et al. (2019). Developments in the mpi-m earth system model version 1.2 (mpi-esm1.2) and its response to increasing co2. *J. Adv. Model. Earth Syst.* 11, 998–1038. doi:10.1029/2018MS001400

Müller, W. A., Jungclaus, J. H., Mauritsen, T., Baehr, J., Bittner, M., Budich, R., et al. (2018). A higher-resolution version of the max planck institute earth system model (mpi-esm1.2-hr). *J. Adv. Model. Earth Syst.* 10, 1383–1413. doi:10.1029/2017MS001217

Nikulin, G., Kjellström, E., Hansson, U., Strandberg, G., and Ullerstig, A. (2011). Evaluation and future projections of temperature, precipitation and wind extremes over europe in an ensemble of regional climate simulations. *Tellus A* 63, 41–55. doi:10.1111/j.1600-0870.2010.00466.x

Outten, S., and Esau, I. (2013). Extreme winds over europe in the ensembles regional climate models. *Atmos. Chem. Phys.* 13, 5163–5172. doi:10.5194/acp-13-5163-2013

Outten, S., and Sobolowski, S. (2021). Extreme wind projections over europe from the euro-cordex regional climate models. *Weather Clim. Extrem.* 33, 100363. doi:10.1016/j.wace.2021.100363

Pryor, S., and Bartelmie, R. J. (2021). A global assessment of extreme wind speeds for wind energy applications. *Nat. Energy* 6, 268–276. doi:10.1038/s41560-020-00773-7

Pryor, S. C., Barthelmie, R. J., Clausen, N. E., Drews, M., MacKeller, N., and Kjellstrom, E. (2012). Analyses of possible changes in intense and extreme wind speeds over northern Europe under climate change scenarios. *Clim. Dyn.* 38, 189–208. doi:10.1007/s00382-010-0955-3

Rockel, B., and Woth, K. (2007). Extremes of near-surface wind speed over europe and their future changes as estimated from an ensemble of RCM simulations. *Clim. Change* 81, 267–280. doi:10.1007/s10584-006-9227-y

Saha, S., Moorthi, S., Pan, H.-L., Wu, X., Wang, J., Nadiga, S., et al. (2010). The ncep climate forecast system reanalysis. *Bull. Am. Meteorological Soc.* 91, 1015–1058. doi:10.1175/2010BAMS3001.1

Schwierz, C., Kollner-Heck, P., Mutter, E., Bresch, D., Vidale, P., Wild, M., et al. (2010). Modelling european winter wind storm losses in current and future climate. *Clim. Change* 101, 485–514. doi:10.1007/s10584-009-9712-1

Séférian, R., Nabat, P., Michou, M., Saint-Martin, D., Voldoire, A., Colin, J., et al. (2019). Evaluation of cnrm earth system model, cnrm-esm2-1: role of earth system processes in present-day and future climate. *J. Adv. Model. Earth Syst.* 11, 4182–4227. doi:10.1029/2019MS001791

Seland, Ø., Bentsen, M., Olivié, D., Toniazzo, T., Gjermundsen, A., Graff, L. S., et al. (2020). Overview of the Norwegian earth system model (noresm2) and key climate response of cmip6 deck, historical, and scenario simulations. *Geosci. Model Dev.* 13, 6165–6200. doi:10.5194/gmd-13-6165-2020

Sellar, A. A., Walton, J., Jones, C. G., Wood, R., Abraham, N. L., Andrejczuk, M., et al. (2020). Implementation of u.k. earth system models for cmip6. *J. Adv. Model. Earth Syst.* 12, e2019MS001946. doi:10.1029/2019MS001946

Smith, D., Scaife, A., Eade, R. e. a., Athanasiadis, P., Bellucci, A., Bethke, I., et al. (2020). North atlantic climate far more predictable than models imply. *Nature* 583, 796–800doi. doi:10.1038/s41586-020-2525-0

Swart, N. C., Cole, J. N. S., Kharin, V. V., Lazare, M., Scinocca, J. F., Gillett, N. P., et al. (2019). The canadian earth system model version 5 (canesm5.0.3). *Geosci. Model Dev.* 12, 4823–4873. doi:10.5194/gmd-12-4823-2019

Tatebe, H., Ogura, T., Nitta, T., Komuro, Y., Ogochi, K., Takemura, T., et al. (2019). Description and basic evaluation of simulated mean state, internal variability, and climate sensitivity in miroc6. *Geosci. Model Dev.* 12, 2727–2765. doi:10.5194/gmd-12-2727-2019

Taylor, K. E., Stouffer, R. J., and Meehl, G. A. (2012). An overview of CMIP5 and the experiment design. *Bull. Am. Meteorological Soc.* 93, 485–498. doi:10.1175/BAMS-D-11-00094.1

Tilo, Z., Andrew, L., Martin, D., Lenton, A., Bodman, R. W., Dix, M., et al. (2020). The Australian earth system model: ACCESS-ESM1.5. *J. South. Hemisphere Earth Syst. Sci.* 70, 193–214. doi:10.1071/ES19035

van der Linden, P., and Mitchell, J. (2009). Climate change and its impacts at seasonal, decadal and centennial timescales. *Tech. Rep*, Met Office Hadley Centre, FitzRoy Road, Exeter EX1 3PB, UK.

Voldoire, A., Saint-Martin, D., Sénési, S., Decharme, B., Alias, A., Chevallier, M., et al. (2019). Evaluation of cmip6 deck experiments with cnrm-cm6-1. *J. Adv. Model. Earth Syst.* 11, 2177–2213. doi:10.1029/2019MS001683

Yang, Y., Wang, B., Cao, J. e. a., and Li, J. (2020). Improved historical simulation by enhancing moist physical parameterizations in the climate system model NESM3.0. *Clim. Dyn.* 54, 3819–3840. doi:10.1007/s00382-020-05209-2

Glossary

AMM	Annual Maximum Method
CFSR	Climate Forecast System Reanalysis
CFDDA	Climate Four-Dimensional Data Assimilation
CMIP5	Fifth Phase of the Coupled Model Intercomparison Project
CMIP6	Sixth Phase of the Coupled Model Intercomparison Project
CORDEX	Coordinated Regional Downscaling Experiment
ECMWF	European Centre for Medium-Range Weather Forecasts
ENSEMBLES	Ensemble-Based Predictions of Climate Changes and Their Impacts
ERA5	5th Generation ECMWF Reanalysis
FINO	Forschungsplattformen in Nord-und Ostsee (Research Platforms in the North Sea and Baltic Sea)
GASP	Global Atlas for Siting Parameters
IEC	International Electrotechnical Commission
IPCC	Intergovernmental Panel on Climate Change
MERRA2	Modern-Era Retrospective Analysis for Research and Applications version 2
PRUDENCE	Prediction of Regional Scenarios and Uncertainties for Defining European Climate Change Risks and Effects
Q_{95} - 95%	percentile of the Wind Speed
RCMs	Regional Climate Models
RCP8.5	Representative Concentration Pathway 8.5
SRES	Special Report on Emissions Scenarios
SSP585	Shared Socioeconomic Pathway 5-8.5
T	Return period in years
U_{50}	50-year Return Period Wind Speed
U_i^{max}	Annual wind maxima
WCRP	World Climate Research Programme
his-Period	Historical Period (1980–2009)
fut-Period	Future Period (2020–2049)
TCL	Turbine Class
SI	Significant Increase
MI	Medium Increase
MD	Medium Decrease
SD	Significant Decrease